PHOTONICS Research

Optically addressed spatial light modulator based on nonlinear metasurface

SHENGCHAO GONG,[1] MENGXIN REN,[1,2,*] WEI WU,[1] WEI CAI,[1] AND JINGJUN XU[1,3]

[1]The Key Laboratory of Weak-Light Nonlinear Photonics, Ministry of Education, School of Physics and TEDA Applied Physics Institute, Nankai University, Tianjin 300071, China
[2]Collaborative Innovation Center of Extreme Optics, Shanxi University, Taiyuan 030006, China
[3]e-mail: jjxu@nankai.edu.cn
*Corresponding author: ren_mengxin@nankai.edu.cn

Received 3 December 2020; revised 8 February 2021; accepted 10 February 2021; posted 12 February 2021 (Doc. ID 416189); published 31 March 2021

Spatial light modulators (SLMs) are devices for modulating amplitude, phase, or polarization of light beams on demand. Such devices are regarded as the backbone for optical information parallel processing and future optical computers. Currently, SLMs are mainly operated in an electrical addressing manner, wherein the optical beams are modulated by electrical signals. However, future all-optical information processing systems prefer to control light directly by light (i.e., optically addressed, OA) without electro-optical conversion. Here, we present an OASLM based on a metasurface (MS-OASLM), whose operation principle relies on nonlinear polarization control of read light by another write light at the nanoscale. Its resolution is more than 10 times higher than a typical commercial SLM and achieves 500 line pairs per millimeter (corresponding to a pixel size of only 1 μm). The MS-OASLM shows unprecedented compactness and is only 400 nm in thickness. Such MS-OASLMs could provide opportunities to develop next generation all-optical information processing and high resolution display technologies.

https://doi.org/10.1364/PRJ.416189

1. INTRODUCTION

Half a century ago, enthusiasm for optical information processing in parallel architectures promoted the invention of spatial light modulators (SLMs) [1–3]. Such devices enable harnessing light in its amplitude, phase, or polarization both spatially and temporally at will [4,5], by which information could be encoded into an optical wavefront with a certain spatial distribution. Nowadays, the SLMs can steadily find themselves in a broad spectrum of applications in our daily lives and cutting edge researches, such as portable displays, virtual reality, light detection and ranging, and super-resolution imaging [6–9].

Depending on the way that information is written into the devices, the SLMs can be divided into electrically addressed SLMs (EASLMs) and optically addressed SLMs (OASLMs) [10]. Complying with the development of electronic information technology during the past decades, the EA has become the most popular technique in current commercial SLMs. However, for future all-optical information process systems, the EASLMs are not the best choice because information needs to convert back and forth between optical and electronic domains. The OASLMs, on the other hand, allow light modulation directly by light without electronic-optical conversion [11,12]. Furthermore, OASLMs are essential for realizing various all-optical applications that are impossible by EASLMs, including coherent to incoherent image conversion, real time optical correlation, and parallel all-optical computation [13–17]. In principle, OASLMs can be constructed based on nonlinearities of materials, in which the modulation over the read light is fulfilled by spatially selectively changing the properties of the materials via nonlinear optical stimuli [2,18–24]. But, the nonlinearities in natural materials are too weak to support efficient "light-control-by-light" within nanoscale volumes. This makes the devices very cumbersome or requires strong pumping power to accumulate sufficiently large nonlinear modulations, and thus such devices are not suitable for the nano-era.

The recent exciting progress in the dynamic optical metasurface (MS) gives an opportunity to tackle the above obstacles and provides a new framework for the nanoscaled SLM [25,26]. The MS can also boost the optical interactions by concentrating light in nanoscale volumes, which makes it possible for significant control over the light fields under, for example, external mechanical, chemical, and magnetic stimuli [27–31]. Based on the active manipulation of light beams by external electrical fields, the ultracompact EASLMs based on MS have been demonstrated recently [25,26,32].

In this paper, we present a novel OASLM based on MS (MS-OASLM). The working principle of our device relies on the nonlinear control of the polarization of the read light by another write light. The MS-OASLM has a ultra-small thickness of only 400 nm, which is thinner than one tenth of any conventional SLMs [4]. Image projections by our MS-OASLM are demonstrated, which are implemented by transforming the polarization modulation into an intensity replica based on Malus' law. The resolution achieves 500 line pairs per millimeter (lp/mm), which is more than one order of magnitude better than the typical commercial SLMs (for example Hamamatsu X10468-01, 25 lp/mm). The MS-OASLM would provide a flexible and compact platform for next generation ultrahigh resolution optical displays and all-optical applications including parallel image processing and parallel optical computing.

2. RESULTS

A schematic of the MS-OASLM is shown in Fig. 1(a). The MS consists of a 100 nm thick metallic nanostructure layer and a spin-coated 300 nm thick ethyl-red azo polymer as a nonlinear switching layer. The unit cells of the metallic nanostructure are composed of L-shaped slits [shown by a scanning electron microscope (SEM) image in the inset], each of which was fabricated via focused ion-beam (FIB) milling through a gold film evaporated on a fused quartz substrate. The nanostructure lattice constant is 300 nm with an entire array footprint of 40 μm × 40 μm. The blue curve in Fig. 1(b) gives the experimentally measured transmission spectrum of the MS with no write light excitation ($P_w = 0$), which shows a resonance dip around 800 nm. Because the unit cells are chiral in geometry, an initially linearly polarized wave [x-polarized in our experiments, output from an acousto-optic filter equipped with a tunable supercontinuum laser (NKT, EXR-15)] would become elliptically polarized with its azimuth rotated after passing through such a medium. The polarization changes are characterized in terms of azimuth rotation ϕ and ellipticity angle χ and measured using a home-built polarimeter [33,34]. The blue trajectory ($P_w = 0$) in Fig. 1(c) gives experimentally measured spectra of ϕ and χ in the wavelength range of 790 to 870 nm without the write light excitation. In our experiment, a green laser (532 nm, CNILASER-MGL-III-532 continuous laser) is adopted as the write light, which stimulates the azo molecules initially in the trans state to convert into the cis state [as shown in Fig. 1(a)]. Such structural isomerization reduces the refractive index of the polymer [35] and consequently changes the resonance conditions of the nanostructures. As a result, blue shifts of both the transmission spectrum [red line in Fig. 1(b)] and ϕ-χ trajectories [Fig. 1(c)] are observed under just a few milliwatts of green light power (P_w). Furthermore, the gradual spectral shift for increased P_w is consistent with the fact that the change of the effective refractive index of the polymer layer is dependent on the pump powers. Up to 10.8° and 9.4° nonlinear changes in ϕ and χ are observed at 820 nm for $P_w = 4$ mW, as presented in Fig. 1(d). This implies that the polarization states of the transmitted light are efficiently varied upon the write light, and Fig. 1(e) intuitively presents the nonlinear changes of the polarization ellipse. Besides, with different pumping power, the refractive index of polymer is also different. It can also be seen from Figs. 1(c)–1(e) that the polarization characters change with different write light powers (P_w).

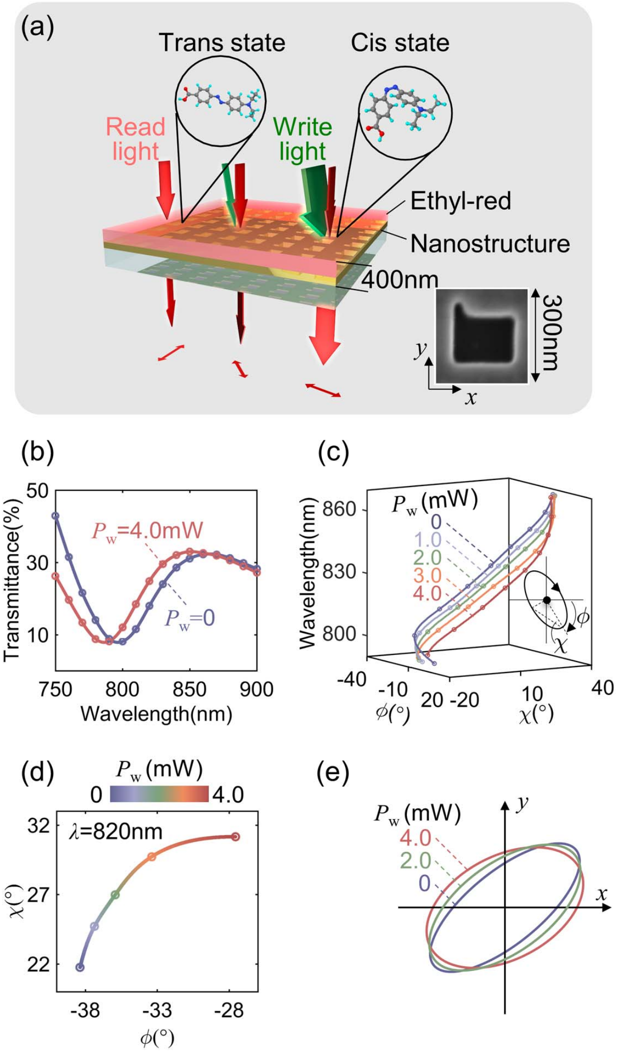

Fig. 1. Operation principle of an MS-OASLM. (a) An illustration for the MS-OASLM. Write beams (green arrows) with different intensities cause a spatially heterogeneous photoisomerization (trans state to cis state) of ethyl-red azo molecules and selectively tune optical responses of the MS. This consequently affects readout light polarization in a nonlinear manner, as indicated by the differently rotated red arrow plane in the transmission side. Inset gives an SEM image of the MS unit cell. (b) Transmission spectra of the MS for x-polarized read light. Irradiation of the write light causes a blue shift of the spectrum (red curve) compared with the initial situation (blue curve). Empty circles are experimental data, and solid lines are eye guides. (c) Nonlinear tuning of the read light polarization as a function of the write light power (P_w). The polarization state of light is defined by azimuth angle ϕ and ellipticity angle χ (defined in inset). Positive values of ϕ and χ correspond to clockwise rotation of polarization azimuth and right-handed ellipse, as observed against propagation direction. Under the write light irradiation, the ϕ-χ trajectory of the read light suffers a blue shift. (d) Modulation over the ϕ-χ curve of the read light at 820 nm. (e) Polarization ellipses of 820 nm read light under different P_w.

Such profound nonlinear polarization effects are sufficient to carry out an OASLM under a write beam. The most wide and fundamental applications of the SLM belong to image

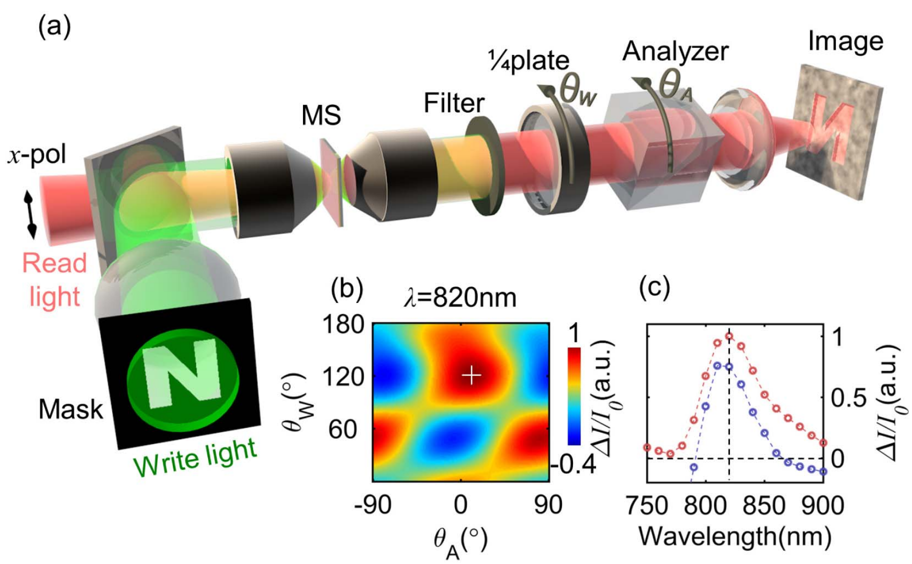

Fig. 2. Image projection based on an MS-OASLM. (a) Schematic of the MS-OASLM image projection system. An input mask is imaged onto the MS plane using 532 nm green light and is duplicated in form of a spatially inhomogeneous polarization distribution in readout light. Such a polarization replica is transformed into an intensity replica by filtering through a combination of a waveplate and a polarizer. (b) Nonlinear intensity modulation ΔI transformed from polarization modulation. θ_W and θ_A are azimuth angles of the waveplate and analyzer, respectively. In the example shown, the wavelength of the read light is 820 nm. The maximum modulation is indicated by a white cross. ΔI is divided by the incident read light intensity (I_0) to get rid of the influence of the power fluctuation of the read laser. (c) Nonlinear modulations to read light intensity at different wavelengths. Blue curve: only contribution from the nonlinear spectral shift in transmitted intensity is considered. For the wavelengths shorter than 790 nm or longer than 860 nm, ΔI is smaller than zero, which gives inverse images of the mask and was not used in our experiments. Red curve: both contributions of nonlinear changes in intensity and polarization are considered, which gives larger ΔI. The strongest modulation appears at 820 nm, to which the results are normalized. Empty circles are experimental data, and dash lines are eye guides.

projection. As a demonstration, an image projecting system was built, as illustrated in Fig. 2(a). The x-polarized read beam was impinged normally onto the MS. A combination of a quarter waveplate and an analyzer was used to translate the nonlinear polarization changes into intensity modulations according to the Malus' law. For a given write light power and a read light wavelength, the read light intensity modulations ΔI are dependent on azimuth angles of waveplate θ_W and analyzer θ_A [33]. As shown in Fig. 2(b), for the example of 820 nm read light, the maximum intensity modulation happens when the waveplate azimuth orients along 121° and the analyzer axis directs along 11°. In order to exclude influence of the power fluctuation of the read laser, the ΔI is further divided by the incident read light intensity (I_0). Figure 2(c) presents the maximum intensity modulations after optimizing θ_W and θ_A at different wavelengths, and it is shown that the largest intensity modulation happens at 820 nm, which is chosen as the read light wavelength in the following image projection experiment. It is worth pointing out that despite the blue shift of the transmission intensity spectrum in Fig. 1(b) inducing nonlinear changes in the transmitted read light intensity [blue curve in Fig. 2(c)], larger ΔI is achieved by further converting polarization modulations into intensity changes by the combination of the quarter waveplate and analyzer based on Malus' law [red line in Fig. 2(c)].

A series of binary masks, which were made by FIB milling transparent letters of "I ♡ N K U" through a 200 nm thick opaque metal film, were put in the green write beam and imaged onto the MS plane by a combination of a lens ($f = 200$ mm) and an objective (10×, N.A. 0.25). In this way, the mask images were duplicated into the polymer layer in form of the spatially heterogeneous isomerization of the azo molecules, which would be further transferred into the spatial polarization variance of the read light. Another objective (10×, N.A. 0.28) was used to collect the transmitted light, and a long pass filter isolated the green light. The read beam was finally photographed onto a complementary metal–oxide–semiconductor (CMOS) camera (Nikon, DS-2MBWc). The final readout images of the letter masks are given in the second row of Fig. 3(a), which present reasonable reproductions of the masks, and the scale bar is given in bottom-right conner.

The spatial resolution is an important parameter of the SLM. The higher resolution refers to the finer modulation over the optical wavefront. The subwavelength sized unit cell not only makes the MS behave as a homogeneous film without optical diffraction, but also theoretically promises ultrahigh resolution with pixel sizes on the wavelength to subwavelength level. To assess the spatial resolution of the MS-OASLM, we replace the letter masks with resolution test charts, which consist of four sets of elements. Each element encloses three horizontal and three vertical lines. The charts are also fabricated by FIB milling through the opaque metal film. The resolution test charts are written onto the MS plane using the green light and form write images with sizes ranging from 20 to 5 μm, as shown in the first and third rows of Fig. 3(b). The readout images by the 820 nm light are given in the second and fourth rows. The elements with sizes of 5 μm are well recognized as

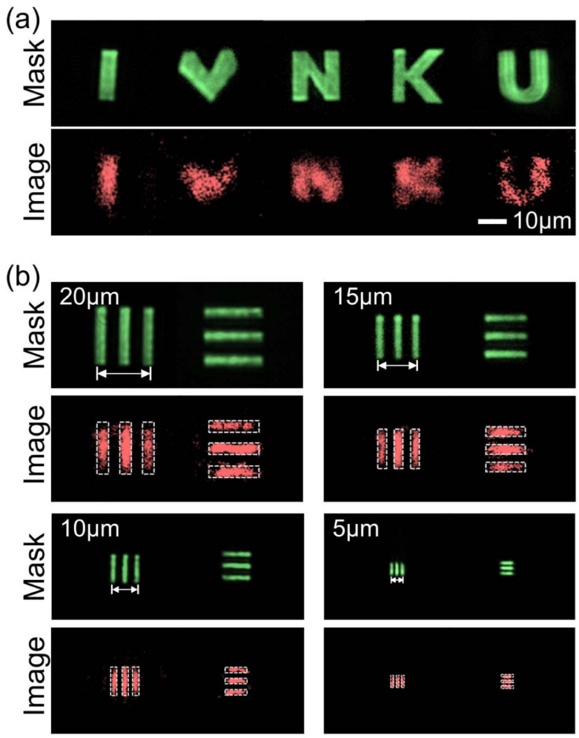

Fig. 3. Read out images of binary masks and resolution test charts. (a) Binary masks include a series of letters, "I ♡ N K U". First row gives optical images of the masks captured directly using green light (532 nm). Images read by the red beam (820 nm) are shown in the second row. Scale bar is 10 μm. (b) Images of different sized resolution test charts by the green light are given in the first and third rows, while images by the read beam are given in the second and fourth rows. The sizes of chart images are labeled beside each pattern. The charts with sizes of 5 μm are well recognized as three distinct lines, corresponding to a spatial resolution of 500 lp/mm.

three distinct lines without any blurring into one another. This implies a spatial resolution of about 500 lp/mm for our OASLM, and the corresponding single pixel size achieves about 1 μm. Such resolution is more than one order of magnitude higher than that of typical commercial SLM devices (for example, Hamamatsu X10468-01, 25 lp/mm) and at least two times larger than that of previously reported liquid crystal (LC)-based OASLMs [2,24,36].

3. CONCLUSION

In conclusion, we demonstrate here a novel ultracompact OASLM based on the nonlinear MS, which fulfills light modulation directly by another write light. Thanks to the outstanding performance of the MS in manipulating light via enhanced nonlinearities at nanoscales, the MS-OASLM acquires a merit of unprecedented compactness with a thickness of about 400 nm, which is less than one tenth of the thickness of the traditional LC-based SLMs. The subwavelength features of the MS make the MS-OASLM free of diffraction in the readout light. In addition, because no LC, electrode, and photosensing layer are needed, our MS-OASLM has a much simpler structure than the traditional LC-SLMs, and can be fabricated simply by standard lithography and spin-coating techniques. Based on our MS-OASLM, we demonstrate the image projection with a high resolution of up to 500 lp/mm, which is more than one order of magnitude higher than typical commercial SLM devices (for example, Hamamatsu X10468-01, 25 lp/mm). Furthermore, such MS-SLMs show advantages of flexibility, i.e., the spectral response of the nanostructures, and hence the read light wavelength of the MS-OASLM, could be easily tuned to any desired spectral range by changing the geometric parameters of the nanostructures. By replacing the traditional bulky optical elements in the projection system with state-of-the-art meta-components, such as metalenses [37], metapolarizers [38], and meta-waveplates [39], the profile of the entire image projection system can be further greatly reduced. Such MS-based OASLMs could find wide applications in novel optical displays and all-optical data parallel processing techniques.

Funding. National Key Research and Development Program of China (2017YFA0305100, 2017YFA0303800, 2019YFA0705000); National Natural Science Foundation of China (92050114, 91750204, 61775106, 11904182, 12074200, 11774185); Guangdong Major Project of Basic and Applied Basic Research (2020B0301030009); Higher Education Discipline Innovation Project (B07013); PCSIRT (IRT0149); Open Research Program of Key Laboratory of 3D Micro/Nano Fabrication and Characterization of Zhejiang Province; Fundamental Research Funds for the Central Universities (010-63201003, 010-63201008, 010-63201009); Tianjin Youth Talent Support Program.

Acknowledgment. We thank the Nanofabrication Platform of Nankai University for fabricating the samples.

Disclosures. The authors declare no conflicts of interest.

REFERENCES

1. J. W. Goodman, *Introduction to Fourier Optics* (Roberts & Company, 1968).
2. D. L. White and M. Feldman, "Liquid-crystal light valves," Electron. Lett. **6**, 837–839 (1970).
3. D. Casasent, *Optical Data Processing: Applications* (Springer-Verlag, 1978).
4. U. Efron, *Spatial Light Modulator Technology: Materials, Devices, and Applications* (Marcel Dekker, 1994).
5. N. Savage, "Digital spatial light modulators," Nat. Photonics **3**, 170–172 (2009).
6. D. Vettese, "Microdisplays: liquid crystal on silicon," Nat. Photonics **4**, 752–754 (2010).
7. A. Maimone, A. Georgiou, and J. S. Kollin, "Holographic near-eye displays for virtual and augmented reality," ACM Trans. Graph. **36**, 85 (2017).
8. J. A. Christian and S. Cryan, "A survey of lidar technology and its use in spacecraft relative navigation," in *AIAA Guidance, Navigation, and Control (GNC) Conference* (2013), paper 4641.
9. Y. M. Sigal, R. Zhou, and X. Zhuang, "Visualizing and discovering cellular structures with super-resolution microscopy," Science **361**, 880–887 (2018).
10. G. Moddel and P. R. Barbier, "Spatial light modulators: processing light in real time," Opt. Photon. News **8**, 17–21 (1997).
11. P. K. Shrestha, Y. T. Chun, and D. Chu, "A high-resolution optically addressed spatial light modulator based on ZnO nanoparticles," Light Sci. Appl. **4**, e259 (2015).

12. P. Chen, L.-L. Ma, W. Hu, Z.-X. Shen, H. K. Bisoyi, S.-B. Wu, S.-J. Ge, Q. Li, and Y.-Q. Lu, "Chirality invertible superstructure mediated active planar optics," Nat. Commun. **10**, 2518 (2019).
13. S. Smith, "Lasers, nonlinear optics and optical computers," Nature **316**, 319–324 (1985).
14. J. Zhang, H. Wang, S. Yoshikado, and T. Aruga, "Incoherent-to-coherent conversion by use of the photorefractive fanning effect," Opt. Lett. **22**, 1612–1614 (1997).
15. M. Shih, A. Shishido, and I. Khoo, "All-optical image processing by means of a photosensitive nonlinear liquid-crystal film: edge enhancement and image addition-subtraction," Opt. Lett. **26**, 1140–1142 (2001).
16. D. Woods and T. J. Naughton, "Optical computing: photonic neural networks," Nat. Phys. **8**, 257–259 (2012).
17. A. Solodar, T. A. Kumar, G. Sarusi, and I. Abdulhalim, "Infrared to visible image up-conversion using optically addressed spatial light modulator utilizing liquid crystal and InGaAs photodiodes," Appl. Phys. Lett. **108**, 021103 (2016).
18. T. Beard, W. Bleha, and S.-Y. Wong, "ac liquid-crystal light valve," Appl. Phys. Lett. **22**, 90–92 (1973).
19. J. Xu, G. Zhang, Q. Wu, Y. Liang, S. Liu, Q. Sun, X. Chen, and Y. Shen, "Holographic recording and light amplification in doped polymer film," Opt. Lett. **20**, 504–506 (1995).
20. A. Grunnet-Jepsen, C. L. Thompson, and W. E. Moerner, "Spontaneous oscillation and self-pumped phase conjugation in a photorefractive polymer optical amplifier," Science **277**, 549–552 (1997).
21. L. Hesselink, S. S. Orlov, A. Liu, A. Akella, D. Lande, and R. R. Neurgaonkar, "Photorefractive materials for nonvolatile volume holographic data storage," Science **282**, 1089–1094 (1998).
22. A. Goonesekera, D. Wright, and W. E. Moerner, "Image amplification and novelty filtering with a photorefractive polymer," Appl. Phys. Lett. **76**, 3358–3360 (2000).
23. Z. Yaqoob, D. Psaltis, M. S. Feld, and C. Yang, "Optical phase conjugation for turbidity suppression in biological samples," Nat. Photonics **2**, 110–115 (2008).
24. K. Miri Gelbaor, K. Matvey, L. Victor, C. Neil, and I. Abdulhalim, "Liquid crystal high-resolution optically addressed spatial light modulator using a nanodimensional chalcogenide photosensor," Opt. Lett. **39**, 2048–2051 (2014).
25. S.-Q. Li, X. Xu, R. M. Veetil, V. Valuckas, R. Paniagua-Domnguez, and A. I. Kuznetsov, "Phase-only transmissive spatial light modulator based on tunable dielectric metasurface," Science **364**, 1087–1090 (2019).
26. J. Li, P. Yu, S. Zhang, and N. Liu, "Electrically-controlled digital metasurface device for light projection displays," Nat. Commun. **11**, 3574 (2020).
27. N. I. Zheludev and Y. S. Kivshar, "From metamaterials to metadevices," Nat. Mater. **11**, 917–924 (2012).
28. M. Kauranen and A. V. Zayats, "Nonlinear plasmonics," Nat. Photonics **6**, 737–748 (2012).
29. G. Li, S. Zhang, and T. Zentgraf, "Nonlinear photonic metasurfaces," Nat. Rev. Mater. **2**, 17010 (2017).
30. X. Duan, S. Kamin, and N. Liu, "Dynamic plasmonic colour display," Nat. Commun. **8**, 14606 (2017).
31. M. Ren, W. Cai, and J. Xu, "Tailorable dynamics in nonlinear optical metasurfaces," Adv. Mater. **32**, 1806317 (2020).
32. J. Park, B. G. Jeong, S. I. Kim, D. Lee, J. Kim, C. Shin, C. B. Lee, T. Otsuka, J. Kyoung, S. Kim, K.-Y. Yang, Y.-Y. Park, J. Lee, I. Hwang, J. Jang, S. H. Song, M. L. Brongersma, K. Ha, S.-W. Hwang, H. Choo, and B. L. Choi, "All-solid-state spatial light modulator with independent phase and amplitude control for three-dimensional lidar applications," Nat. Nanotechnol. **16**, 69–76 (2020).
33. M. Ren, M. Chen, W. Wu, L. Zhang, J. Liu, B. Pi, X. Zhang, Q. Li, S. Fan, and J. Xu, "Linearly polarized light emission from quantum dots with plasmonic nanoantenna arrays," Nano Lett. **15**, 2951–2957 (2015).
34. M.-X. Ren, W. Wu, W. Cai, B. Pi, X.-Z. Zhang, and J.-J. Xu, "Reconfigurable metasurfaces that enable light polarization control by light," Light Sci. Appl. **6**, e16254 (2017).
35. T. Lückemeyer and H. Franke, "Nonlinear and bistable properties of doped PMMA lightguides," Appl. Phys. A **55**, 41–48 (1992).
36. S. Fukushima, T. Kurokawa, and M. Ohno, "Real-time hologram construction and reconstruction using a high-resolution spatial light modulator," Appl. Phys. Lett. **58**, 787–789 (1991).
37. M. Khorasaninejad, W. T. Chen, R. C. Devlin, J. Oh, A. Y. Zhu, and F. Capasso, "Metalenses at visible wavelengths: diffraction-limited focusing and subwavelength resolution imaging," Science **352**, 1190–1194 (2016).
38. Y. Chen, J. Gao, and X. Yang, "Direction-controlled bifunctional metasurface polarizers," Laser Photon. Rev. **12**, 1800198 (2018).
39. Y. Zhao and A. Alu, "Tailoring the dispersion of plasmonic nanorods to realize broadband optical meta-waveplates," Nano Lett. **13**, 1086–1091 (2013).